HHS Public Access

Author manuscript

Neuroimage. Author manuscript; available in PMC 2017 April 01.

Published in final edited form as:

Neuroimage. 2016 April 1; 129: 260–267. doi:10.1016/j.neuroimage.2016.01.010.

Intrinsic connectivity of neural networks in the awake rabbit

Matthew P Schroeder[a], **Craig Weiss**[a], **Daniel Procissi**[b], **John F. Disterhoft**[#a], and **Lei Wang**[#b,c]

[a] Department of Physiology, Feinberg School of Medicine, Northwestern University, 303 E. Chicago Avenue, Ward Building 7-140, Chicago, Illinois 60611, USA

[b] Department of Radiology, Feinberg School of Medicine, Northwestern University, 737 North Michigan Avenue, Suite 1600, Chicago, IL 60611, USA

[c] Department of Psychiatry and Behavioral Sciences, Feinberg School of Medicine, Northwestern University, 710 N. Lake Shore Drive, Abbott Hall 1322, Chicago, IL 60611, USA

[#] These authors contributed equally to this work.

Abstract

The way in which the brain is functionally connected into different networks has emerged as an important research topic in order to understand normal neural processing and signaling. Since some experimental manipulations are difficult or unethical to perform in humans, animal models are better suited to investigate this topic. Rabbits are a species that can undergo MRI scanning in an awake and conscious state with minimal preparation and habituation. In this study, we characterized the intrinsic functional networks of the resting New Zealand White rabbit brain using BOLD fMRI data. Group independent component analysis revealed seven networks similar to those previously found in humans, non-human primates and/or rodents including the hippocampus, default mode, cerebellum, thalamus, and visual, somatosensory, and parietal cortices. For the first time, the intrinsic functional networks of the resting rabbit brain have been elucidated demonstrating the rabbit's applicability as a translational animal model. Without the confounding effects of anesthetics or sedatives, future experiments may employ rabbits to understand changes in neural connectivity and brain functioning as a result of experimental manipulation (e.g., temporary or permanent network disruption, learning-related changes, drug administration, etc.).

Graphical Abstract

Corresponding author: Lei Wang, 710 N. Lake Shore Dr. Abbott Hall 1322, Chicago, IL 60611, leiwang1@northwestern.edu, (312) 503-3983.
mp.schroeder@u.northwestern.edu
cweiss@northwestern.edu
d-procissi@northwestern.edu
jdisterhoft@northwestern.edu

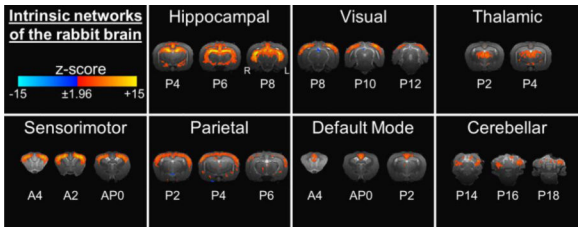

Keywords

Functional magnetic resonance imaging; Default Mode Network; Awake animal MRI; Independent component analysis; Functional connectivity

1. Introduction

The brain constantly transmits neural signals among various regions whether during idle wakefulness (i.e., “at rest”) or different behavioral states like cognitively-demanding tasks (Baldassarre et al., 2012; Hampson et al., 2006; Tambini et al., 2010). Studies using functional magnetic resonance imaging (fMRI) in humans, non-human primates, and rodents have consistently observed neural networks of coherent activity within and between brain structures subserving some functional purpose or neuronal processing (Beckmann et al., 2005; Belcher et al., 2013; Hutchison et al., 2011; Lu et al., 2012; Mantini et al., 2013; Power et al., 2011; Shirer et al., 2012). These neural networks appear malleable as a function of development (Betzel et al., 2014; Greene et al., 2014; Pizoli et al., 2011; Power et al., 2010) or cognitive training (Lewis et al., 2009; Mackey et al., 2013).

The ability to collect imaging data during a resting, wakeful state eliminates the potential confounds associated with task-related performance in clinical populations. Intrinsic network connectivity measures have the potential to determine the potential efficacy of treatment (Fox et al., 2012) and might provide biomarkers for the identification of specific abnormal brain function related to psychiatric disease (Fox and Greicius, 2010). Robust differences in intrinsic network connectivity have been seen between healthy controls and individuals with ADHD (Fair et al., 2012; McLeod et al., 2014), neurodegenerative and Alzheimer's disease (Damoiseaux et al., 2012; Greicius et al., 2004; Lehmann et al., 2013; Lustig et al., 2003; Seeley et al., 2009; Supekar et al., 2008), schizophrenia (Yu et al., 2012), Tourette's (Church et al., 2009), or Fragile × syndrome (Hall et al., 2013).

Animal models serve a useful purpose to study the phenomena of intrinsic connectivity as some experimental manipulations are difficult or unethical to perform in humans (e.g., temporary or permanent lesioning of neural hubs). However, many animal models require sedation or anesthesia to be imaged which can significantly alter functional networks (Boveroux et al., 2010; Brevard et al., 2003; J. V Liu et al., 2013; X. Liu et al., 2013). Identifying animal models that can be imaged in an awake and conscious state in order to preserve intrinsically active neural networks allows for greater translatability to humans.

The rabbit is an ideal and unique animal model for the study of intrinsic connectivity due to their ability to be imaged while in a docile awake state without the need for any sedation or

anesthetic agents, their tolerance for restraint (Li et al., 2003; Wyrwicz et al., 2000), and their adaptations to living in narrow underground burrows. A relatively simple surgery to implant an atraumatic restraining headpost assembly allows the rabbit to remain in a standard stereotaxic orientation thus minimizing movement of the head and brain and preventing image artifacts and distortion. A single day of habituation to the MRI and gradient sequence provides sufficient acclimation to the environment (Wyrwicz et al., 2000).

In this study, we characterize the intrinsic connectivity networks of the rabbit brain for the first time. Group independent component analysis revealed seven networks related to the hippocampus, default mode, cerebellum, thalamus, and visual, somatosensory, and parietal cortices that are similar to previously observed networks in humans, non-human primates and/or rodents. Understanding the neural networks of the rabbit brain will provide an additional translational animal model to probe alterations in functional connectivity as a consequence of experimental manipulation, drug administration or disease states/agents without the confounding factors of anesthesia or sedation.

2. Methods

2.1 Subjects and surgery

Twelve female, New Zealand White rabbits (2-4kg) were used in the current study. Surgery was performed under NIH and Northwestern University IACUC approved protocols to implant a restraining bolt assembly onto the rabbit's skull in order to fix the head in our custom-built MR cradle. Anesthesia was induced with ketamine (60 mg/kg, i.m.) and xylazine (10 mg/kg, i.m.). Buprenex (0.03 mg/kg, s.c.) was administered to minimize discomfort during and after the procedure and ophthalmic ointment was applied to keep the eyes moist. After rabbits were placed into a stereotaxic apparatus, the scalp was incised and the skull was positioned with lambda 1.5mm below bregma. In order to secure the headpost onto the skull in the stereotaxic plane (Girgis and Shih-Chang, 1981; Sawyer et al., 1954), six holes (four rostral to bregma and two lateral to lambda) were drilled into (but not through) the skull. Nylon machine screws were turned into holes threaded with a 2-56 bottoming tap. After Grip cement (Dentsply) was placed on the skull and machine screws, a custom-built headpost assembly (four upright nylon bolts (6-32 × 3/4″)) encased in Grip cement) was lowered onto the cement-covered skull. Additional cement was added as necessary to secure the headpost assembly and cover the skull. Metacam (0.2 mg/kg, s.c.) was administered once the rabbits were sternal and again 24 hours later to provide analgesia. Grip cement did not induce any susceptibility artifacts in EPI images (Supplementary Fig. 1).

2.2 Animal restraint for resting-state fMRI

After one week of post-operative recovery (i.e., to insure that normal eating, drinking, and activity returned), rabbits underwent a one-day habituation protocol to the MRI scanner environment. For habituation and all subsequent scanning, earplugs were inserted and rabbits were placed in a prone position inside a cotton wrap and a canvas bag (Lomir) secured with Velcro. A single-channel, receive-only RF surface coil was secured to the underside of a Plexiglas crossbar and secured onto the rabbit's headpost with four nylon

nuts. The crossbar was fastened to the custom-built cradle to stabilize the rabbit's head and prevent movement. With the headposted rabbit fixed inside the cradle, it was placed in the MR scanner. A one hour EPI sequence was performed to fulfill habituation training. Repositioning of the same animal was achieved in all three directions (X, Y, and Z) with great accuracy (<500 um) across sessions. The configuration of the custom-built cradle with the single-channel, receive-only RF surface coil is presented in Supplementary Figure 2.

Criterion for habituation was achieved after a single session. By visualizing the EPI images in real-time, no signs of excessive movement (i.e., > 0.3mm) lasting longer than 2 repetition times (i.e., 5s) occurred during the habituation protocol. Although we did not collect any measurement to ascertain the stress of the rabbit (e.g., corticosterone levels), rabbits did not display any signs of overt stress (i.e., struggling) and direct monitoring of the digital waveform generated by a respiration pillow revealed consistent and maintained breathing patterns not interrupted by any excessive movement throughout the duration of scanning.

2.3 MRI data acquisition

MR scanning was conducted in a Bruker 7T/30cm wide horizontal magnet (ClinScan, Bruker Biospin, Ettlingen, Germany) using Syngo VB15 platform from Siemens. Transmission was achieved with a two channel volume coil fixed inside the magnet with a single-channel, receive-only RF surface coil with an inner diameter of 30mm. A single anatomical and functional scan were acquired once per day for seven consecutive days. An anatomical reference image was first acquired using a gradient echo sequence with the following geometrical and MR parameters: 1.0mm slice thickness (40 slices), 0.5 × 0.5mm in-plane resolution, FOV = 64 × 64mm, matrix size = 128 × 128 × 40, TR = 500ms, TE = 2.09ms, flip angle = 90°. Blood-oxygen-level dependent (BOLD) contrast-sensitive T_2*-weighted gradient-echo echo-planar images (EPI) covering the entire rabbit brain were acquired for intrinsic connectivity scans (200 volumes, 20 coronal slices, repetition time (TR) = 2.5s, echo time (TE) = 25ms, total bandwidth = 367kHz, flip angle = 90°, 2.0mm slice thickness, 0.5 × 0.5 mm in-plane resolution, FOV = 35 × 26mm; matrix size = 70 × 52 × 20, 200 volumes, total time = 8:20). Adjustments to optimize shimming, reduce air-tissue artifacts and produce a uniform magnetic field were performed on a manually selected region (centered on, but not exceeding the size of, the rabbit brain). First and second order shimming was performed using an automated field map algorithm included in the Syngo platform. Shim tables showing the resulting x, y, z and higher order shim values confirmed no major variability in shim values across subjects and sessions.

2.4 fMRI data analysis

Data analysis was performed with AFNI (Cox, 1996) and FSL (Beckmann and Smith, 2004). The first three volumes of each dataset were discarded to account for eddy currents and NMR equilibrium. After performing slice-timing and motion correction, displacement of each brain volume relative to the previous volume was calculated as the Euclidian norm of the translational (x, y, z) and rotational (α, β, γ) rigid-body motion correction parameters (displacement = square root of $[(\Delta x)^2 + (\Delta y)^2 + (\Delta z)^2 + (\Delta\alpha)^2 + (\Delta\beta)^2 + (\Delta\gamma)^2]$ (Belcher et al., 2013). Rotational displacements were converted from radians to millimeters by calculating displacement on the surface of a sphere of radius 14 mm (about the mean

distance from the cerebral cortex to the center of the head). Since rotational or translational displacement did not exceed our criterion of 0.3 mm, no data points were eliminated due to excessive motion. The average maximum displacement across the entire subject population was 0.11 mm (s.d. = 0.07 mm). EPI images from each rabbit were co-aligned with the anatomical reference scan collected during the same session. Anatomical scans were then spatially aligned to a separate, previously collected, high-resolution rabbit brain ($0.2mm^3$ resolution). Output from coregistration procedures demonstrated no significant issues and based on our semi-quantitative estimates, we are confident of the spatial accuracy in coregistered images. The same transformation was applied to the EPI images and the original voxel resolution (2.0 × 0.5 × 0.5mm) was kept. Additional preprocessing steps included regression of motion parameters, temporal filtering (0.005-0.1Hz), and spatial smoothing (FWHM = 0.71 mm).

For each of the rabbit's seven intrinsic connectivity scans, voxels were divided by their mean signal intensity and concatenated. Group-level independent component analysis was performed using the FSL program MELODIC (Multivariate Exploratory Linear Optimized Decomposition into Independent Components). MELODIC uses independent component analysis to linearly decompose multiple 4D data sets into a set of spatial maps (i.e., independent components) without the need to specify any explicit time series model. Using an unconstrained model, 56 independent components were identified. However, visualization of each component revealed splitting of putative bilateral networks into unilateral ones. As a result, we performed exploratory analyses with models specifying 15, 18, 21, 24, 27, and 30 components and ultimately chose the model with 24 components due to the bilaterality of components and their similarity to previously described networks in humans, non-human primates (rhesus and marmoset monkeys), and rodents (Beckmann et al., 2005; Belcher et al., 2013; Hutchison et al., 2011; Lu et al., 2012; Mantini et al., 2013; Shirer et al., 2012). For each component, MELODIC produced a z-score for each voxel measuring the standard deviation from the mean voxel-specific background noise as estimated by a Gaussian-Gamma mixture model fit (Beckmann and Smith, 2004). Determination of putative network labels for the physiologically relevant components was based on relevant rabbit brain atlases and journal articles (Girgis and Shih-Chang, 1981; Gould, 1986; Hughes and Vaney, 1982; Urban and Richard, 1972).

A seed-based approach was also employed to verify the components. Using a 2mm spherical ROI at the voxel with the highest z-score within the component, reference time courses were created by averaging all voxels within the ROI and cross-correlating with the entire brain. Z-transformed correlation maps were subjected to a t-test against zero to determine significance and thresholded at a corrected p-value <.05 (individual voxel threshold= $p < .001$ with a minimum cluster size of 5 voxels).

To determine within-subject reliability and across-subject robustness, spatial and temporal regression (i.e., dual-regression in FSL (Filippini et al., 2009)) was performed on each of the seven scans for each rabbit to produce a subject-session-specific component map based on the group-level component maps. The degree of between-network coherence was calculated by cross-correlating each of the seven components time-courses within each rabbit, applying Fisher z-transformations and subjecting each of the 21 comparisons to a t-test against zero

(corrected for multiple comparisons). The degree of spatial overlap between the subject-session-specific component maps and the group-level component map was calculated using a voxel-wise spatial correlation method. The subject's spatial correlation coefficients from the seven sessions were subjected to a maximum normed residual test (i.e., Grubbs' test) to detect significant outliers ($p>.05$).

3. Results

Of the 24 components produced using MELODIC group ICA, 17 were related to CSF, white matter, or physiological/scanner artifacts and were not analyzed further (see Supplementary Figures 3-4). The remaining 7 components (i.e., networks) were related to the hippocampus, default mode, cerebellum, thalamus, and visual, somatosensory, and parietal cortices. The 7 components accounted for 30.7% of the variance within the data with each component ranging in explained variance from 3.6 - 5.7%. Table 1 lists the components in the rank order of explained signal variance and Figure 1 shows functional data overlaid on the previously collected, high-resolution anatomical scan that served as our alignment template.

The greatest amount of variance is explained by the hippocampal component (C1) which also includes the caudal anterior cingulate (cACC), prelimbic cortex (located medially at A6-A8), dorsomedial (MD) thalamus (located at P2), and insula (located medially and ventrolaterally, respectively, at A2) (Fig. 1A). Component C2 encompasses visual areas V1 and V2 (Fig. 1B) and component C3 includes the thalamus (Fig. 1C).

Component C4 is identified as the sensorimotor network (Fig. 1D) which is similar to previous studies in humans and monkeys (Beckmann et al., 2005; Belcher et al., 2013; Damoiseaux et al., 2006; Hutchison et al., 2011; Mantini et al., 2013; Shirer et al., 2012). Component C5 includes the parietal cortical network (Fig. 1E) which also includes the auditory cortex. The parietal network appears more lateral and caudal compared to the sensorimotor network (Fig. 1D) and is prominently seen from bregma (AP0) to 6 mm posterior to bregma (P6).

Component C6 extends anterior towards the prefrontal cortex and is identified as the default mode network (DMN) in the rabbit given its similarity to the same network in rodents (Lu et al., 2012), non-human primates (Belcher et al., 2013; Hutchison et al., 2011; Vincent et al., 2007), and humans (Buckner et al., 2008; Smith et al., 2012) (Figures 1F and 2). Finally, we identified a network related to the cerebellum, C11, which is bilateral and includes the anterior most part of the ansiform lobe and the dorsal most part of the superior cerebellar peduncle (the output fibers from the cerebellar deep nuclei) (Fig. 1G).

Our initial seed-based approach to verify the components revealed that the hippocampus and cortex were included in all of the seven seed-based maps (Supplementary Figure 5). The hippocampus and cortex, being relatively close to the receive-only surface coil and having high relative SNR, appeared to dominate the signal within the datasets causing significant correlations within each seed-based analysis. As a result, we regressed out the average signal from the four cortical seeds (i.e., DMN, visual, somatosensory, and parietal cortex) and reperformed the seed-based analysis with the hippocampus as an ROI. Additionally, we

regressed out the average signal from the hippocampal seed and reperformed our seed-based analysis with the six non-hippocampal components (Supplementary Figure 6). The resulting seed-based maps largely recapitulate the spatial maps of their respective independent components suggesting that the ICA approach effectively overcomes the issues relating to variable SNR as a function of distance from the surface coil to identify distinct, anatomically-relevant independent components.

Figure 3 examines the degree of coherence between each pair of the 7 networks. Nearly all of the 21 comparisons were significantly different from zero. Those that were not significant include the comparisons to the cerebellum and visual/default mode network with the thalamic network. The DMN shows the highest coherence with the hippocampus to which it is functionally connected (Berger et al., 1980; Shibata and Honda, 2012). Interestingly, the thalamic network has weak to moderate coherence with each network ($Z < 0.290$).

To validate the inter-subject reliability and robustness of the 7 components, the seven intrinsic connectivity scans from each rabbit were subjected to dual-regression to produce subject-session-specific component maps. No significant outliers were detected in the spatial overlap between the dual-regression derived component maps and the group-level component map confirming the reliability of component detection and emphasizing their physiological relevance. In fact, the standard deviation of the spatial overlap across the seven sessions in our twelve rabbits was relatively small ranging from 0.006 to 0.047 (means of the seven components ranged from .250 to .645, average coefficient of variation=4.30%; Fig. 4). The average Z-transformed spatial correlation between subject-specific component maps and the group-level component map varied between 0.329 and 0.481 (average standard deviation across the seven components = 0.056) indicating some variation in spatial correlation values across the twelve rabbits.

4. Discussion

We report that seven physiologically relevant intrinsic networks exist in the awake and conscious rabbit brain which agree with previous reports in humans, non-human primates, and rodents.

4.1 Comparison of networks with other species

While the possibility exists that ICA methodology did not sufficiently separate the data to produce a hippocampal-only network, our hippocampal network (Fig. 1A) is consistent with previous reports in rodents and non-human primates (Becerra et al., 2011; Hutchison et al., 2011, 2010; Jonckers et al., 2011). Further, that prelimbic cortex and MD thalamus exhibited coherence with this network is consistent with the fact that reciprocal projections exist between the two regions in the rabbit and rat (Buchanan, 1994; Kuroda et al., 2004). Human studies tend to identify the hippocampus as part of the larger default mode network (DMN) rather than as a component by itself (Greicius et al., 2004). In contrast, intrinsic hippocampal networks in rodents and macaques are identified as separate networks (Becerra et al., 2011; Hutchison et al., 2011, 2010; Jonckers et al., 2011) as we have found.

The DMN, which exhibits deactivation during goal-oriented behavior and is thought to relate to introspective thinking and remembering about the past, is one of the most robust and reliable networks in the human brain (Buckner et al., 2008; Raichle et al., 2001) being composed of the posterior cingulate, parietal cortex, medial prefrontal cortex, and the hippocampus (Greicius et al., 2004). The DMN has also been characterized in non-human primates and rats (Belcher et al., 2013; Hutchison et al., 2011; Lu et al., 2012; Mantini et al., 2011) whereas the DMN of rabbits (Fig. 1F), which includes the homologue of the posterior cingulate in humans (retrosplenial cortex), is more visually similar to the DMN observed in rodents (see Figure 1 of Lu et al., 2012 for comparison of rat, monkey, and human DMN). Examining the coherence of the DMN with the hippocampal network (another region involved in the DMN in humans) reveals high coherence between the two (0.530; Fig. 3).

The sensorimotor network (Fig. 1D) bears high correspondence with multi-unit electrophysiological recording studies performed in rabbits which localize the primary somatosensory cortex from ~4mm anterior to bregma (~A4) to 2mm posterior to bregma (~P2) (Gould, 1986). This network is prominent in human, rodent, and monkey resting-state studies (Becerra et al., 2011; Beckmann et al., 2005; Belcher et al., 2013; Buckner and Vincent, 2007; Hutchison et al., 2011; Jonckers et al., 2011; Liang et al., 2011; Mantini et al., 2013).

Previous work in rodents has shown subregional thalamic connectivity to its anatomical projections (Becerra et al., 2011), whereas our thalamic network is primarily composed of a single component (the MD thalamus is also involved with the hippocampal component (Fig. 1A)). Because distinct thalamic nuclei serve as relays between the prefrontal cortex and cerebellum (Kelly and Strick, 2003; Weiss and Disterhoft, 2011) as well as between cortical-cortical connections (Shibata and Honda, 2012), the thalamic network may be functionally connected to all of the networks some of the time as opposed to a single network all of the time. Human ICA studies often fail to identify the thalamus as an independent network, although seed-based analyses show reliable connectivity of a subsection of the thalamus to the entirety of the thalamus (Stein et al., 2000).

The cerebellum contains a fractured somatotopy (Shambes et al., 1978) with multiple somatomotor representations and is connected to the cerebral cortex by way of polysynaptic circuits (Evarts and Thach, 1969; Kemp and Powell, 1971; Schmahmann and Pandya, 1997; Strick, 1985). Seed-based approaches suggest a complex topography of subregional cerebellar connectivity with distinct cortical areas (Buckner et al., 2011) while human studies using ICA have identified the cerebellum as a single network of reliable coherent activity (Dobromyslin et al., 2012; Smith et al., 2009) similar to our analysis (Fig. 1G). Although the significant regions located in slice P12 do not appear to be within the cerebellum, this is likely due to our large anterior-posterior voxel size (i.e., 2mm).

Small, but statistically significant negative clusters (i.e., BOLD signals modulated opposite or off-phase to that of the independent component time-course) can be seen in 2 of the 7 components near the third ventricle (Fig. 1B) and borders of the brain (Fig. 1E). These clusters were rare and small when present (respectively account for 2.78% and 2.93% of the total amount of significant voxels in these components). Subject movement during

acquisition can confound resting state networks but movement artifacts do not seem to be related to our components. In correlating each component time course to each of the six motion parameters, the average of the absolute correlation values is 0.005 (range = −0.012 to 0.009) suggesting movement is not associated with our components. Other artifacts such as susceptibility artifacts and pulsation) can also confound resting state networks which may explain the small negative clusters observed in our parietal and visual networks.

Because our data collection employed a single channel surface coil, we do not see as many subcortical networks as compared to previous studies. Among the networks commonly seen in other studies but absent in ours is the basal ganglia, executive control, and frontoparietal networks. As can be seen in Supplementary Figure 1, our signal-to-noise ratio (SNR) in subcortical structures is diminished compared to structures closer to the surface coil. Also, the use of a surface coil may also contribute to the seemingly high coherence values between networks (Fig. 3). We know of no comparable literature to assess whether the degree of coherence strength between our component time courses is indeed elevated. We are currently in the process of adapting a 4-channel coil to be used in the rabbits with the aim of improving SNR, identifying subcortical networks in the rabbit brain, collecting higher resolution anatomical and functional images as well as investigating inter-network coherence strength.

In our initial seed-based approach to verify the components (Supplementary Figure 5A-F), the hippocampus and regions of the cortex appear in nearly every analysis. Once the hippocampus or cortex was regressed out, the spatial maps largely resembled those of their respective independent components (Supplementary Figure 6A-F). The use of a surface coil for signal reception enhances the SNR for regions in close proximity to the coil such as the hippocampus and cortex (as depicted in Supplementary Figure 1). While the entire hippocampus is identified as a single component in our analysis (Figure 1A) which has a single time course that identifies its variation in our data, the cortex is comprised of four components each with their own time course explaining variation in our data. When the average signal from the four cortical seeds are regressed out, our hippocampal seed-based analysis highlights a more refined hippocampal network (Supplementary Figure 6A). Conversely, regressing out the signal from the hippocampus and examining each of the four cortical networks replicates the findings from the ICA analysis (Supplementary Figure 6B-F). Because ICA splits dominant modes of variation into separate components, our ICA analysis was able to overcome the issues related to SNR to first identify a hippocampal network and then identify networks of the brain that explain additional variance (such as the sensorimotor, visual, parietal, cerebellar cortex as well as thalamic and default mode network).

As this is the first examination of the intrinsic networks of the rabbit brain, future experiments are underway to examine the effect of anesthesia on intrinsic connectivity in the rabbit using a within-subjects design. In addition, behavioral experiments are planned in which rabbits will be trained on a hippocampal-dependent task (i.e., trace eyeblink conditioning) and connectivity measures will be assessed at various points in the learning process to assess alterations within and between networks. Finally in order to localize findings to a standard template, we use the atlas of Girgis and Shih-Chang (1981) which we

have found to be very accurate when examining histology, and we plan to use an MRI-based atlas to automatically parcellate significant results (Muñoz-Moreno et al., 2013).

4.2 Rabbit is a translational animal model to study intrinsic connectivity

Rabbits represent a unique and ideal translational animal model for basic neuroimaging research and translational drug discovery and is bolstered by a rich publication history using single and multi-unit neuron recordings (Christian and Thompson, 2003; Hattori et al., 2014a, 2014b; Medina et al., 2002). Many of the functional networks we observed in rabbits resemble those found in humans, and rabbits have several advantages: the rabbit brain size exceeds those of rodents (thus facilitating imaging and electrophysiological experiments), minimal preparation and habituation is required, and the rabbit does not require any anesthetic agent or sedation for fMRI experiments. Although rodents are easy to manipulate and are the most commonly used laboratory species, they generally require anesthesia to remain motionless in the MR scanner which has been shown to significantly disrupt inter-regional connectivity (Boveroux et al., 2010; Brevard et al., 2003; J. V Liu et al., 2013; X. Liu et al., 2013). Sedative agents such as medetomidine limit the effects on the natural BOLD signal, but questions still exist regarding its role in disrupting neural synchrony (Nasrallah et al., 2012). Alternatively, imaging awake rodents preserves the BOLD signal, but often requires extensive training for them to adapt to restraint. Non-human primates are the best homologue to humans due to their closer evolutionary link, but face significant ethical, practical, and financial challenges in using them for imaging research.

4.3 Employing animal models to study disruptions to neural network hubs

Studies that permanently or temporarily lesion network hubs may lead to a better understanding of the behavioral and functional disturbances that occur as a result of the lesion or disease states. In order to examine how disrupting hubs of neural activity can alter the brain's intrinsic connectivity, animal models can bypass many of the experimental and ethical constraints posed on humans (O'Reilly et al., 2013). Initially, a lesion will disrupt structural networks followed by compensatory effects and readjustments on functional connections (Sporns, 2014), but the behavioral effects may depend on the neural region being lesioned. Peripheral, non-hub lesions will produce specific behavioral deficits, whereas lesions of hub regions will have a much greater impact on behavior (Pessoa, 2014). With our results highlighting the utility of the rabbit as an additional translational animal model, questions regarding the effects of network disruption may start to be answered in vivo.

5. Conclusions

This study is the first investigation of the intrinsic network connectivity in the resting rabbit brain with fMRI. Many of the same networks found in humans, non-human primates, and rodents are also found in the rabbit. Our findings provide the first examination of the rabbit as a potential animal model for translational research studying neural networks and provide the baseline data for changes that may occur during different behavioral states or disease states such as Alzheimer's disease (Deci et al., 2012; Liu et al., 2012; Perez-Garmendia et al., 2014; Schreurs et al., 2013).

Supplementary Material

Refer to Web version on PubMed Central for supplementary material.

Acknowledgements

This work was supported by the National Institutes of Health (National Institute of Neurological Disorders and Stroke Grant NS059879 to CW and the National Institute of Mental Health Grant MH47340 to JFD). M.S. was supported by the T32 Training Program: The Neuroscience of Human Cognition at Northwestern University (T32-NS047987).

We thank Jay Gottfried and Ken Paller for their valuable contributions and suggestions for this manuscript.

References

Baldassarre A, Lewis CM, Committeri G, Snyder AZ, Romani GL, Corbetta M. Individual variability in functional connectivity predicts performance of a perceptual task. Proc. Natl. Acad. Sci. U. S. A. 2012; 109:3516–21. doi:10.1073/pnas.1113148109. [PubMed: 22315406]

Becerra L, Pendse G, Chang P-C, Bishop J, Borsook D. Robust reproducible resting state networks in the awake rodent brain. PLoS One. 2011; 6:e25701. doi:10.1371/journal.pone.0025701. [PubMed: 22028788]

Beckmann CF, DeLuca M, Devlin JT, Smith SM. Investigations into resting-state connectivity using independent component analysis. Philos. Trans. R. Soc. Lond. B. Biol. Sci. 2005; 360:1001–13. doi: 10.1098/rstb.2005.1634. [PubMed: 16087444]

Beckmann CF, Smith SM. Probabilistic independent component analysis for functional magnetic resonance imaging. IEEE Trans. Med. Imaging. 2004; 23:137–52. doi:10.1109/TMI.2003.822821. [PubMed: 14964560]

Belcher AM, Yen CC, Stepp H, Gu H, Lu H, Yang Y, Silva AC, Stein EA. Large-scale brain networks in the awake, truly resting marmoset monkey. J. Neurosci. 2013; 33:16796–804. doi:10.1523/JNEUROSCI.3146-13.2013. [PubMed: 24133280]

Berger TW, Milner TA, Swanson GW, Lynch GS, Thompson RF. Reciprocal anatomical connections between anterior thalamus and cingulate— retrosplenial cortex in the rabbit. Brain Res. 1980; 201:411–417. doi:10.1016/0006-8993(80)91044-6. [PubMed: 6774801]

Betzel RF, Byrge L, He Y, Goñi J, Zuo X-N, Sporns O. Changes in structural and functional connectivity among resting-state networks across the human lifespan. Neuroimage 102 Pt. 2014; 2:345–57. doi:10.1016/j.neuroimage.2014.07.067.

Boveroux P, Vanhaudenhuyse A, Bruno M-A, Noirhomme Q, Lauwick S, Luxen A, Degueldre C, Plenevaux A, Schnakers C, Phillips C, Brichant J-F, Bonhomme V, Maquet P, Greicius MD, Laureys S, Boly M. Breakdown of within- and between-network Resting State Functional Magnetic Resonance Imaging Connectivity during Propofol-induced Loss of Consciousness. Anesthesiology. 2010; 113:1038–53. doi:10.1097/ALN.0b013e3181f697f5. [PubMed: 20885292]

Brevard ME, Duong TQ, King JA, Ferris CF. Changes in MRI signal intensity during hypercapnic challenge under conscious and anesthetized conditions. Magn. Reson. Imaging. 2003; 21:995–1001. [PubMed: 14684202]

Buchanan SL. Mediodorsal thalamic lesions impair acquisition of an eyeblink avoidance response in rabbits. Behav. Brain Res. 1994; 65:173–9. [PubMed: 7718150]

Buckner RL, Andrews-Hanna JR, Schacter DL. The brain's default network: anatomy, function, and relevance to disease. Ann. N. Y. Acad. Sci. 2008; 1124:1–38. doi:10.1196/annals.1440.011. [PubMed: 18400922]

Buckner RL, Krienen FM, Castellanos A, Diaz JC, Yeo BTT. The organization of the human cerebellum estimated by intrinsic functional connectivity. J. Neurophysiol. 2011; 106:2322–45. doi:10.1152/jn.00339.2011. [PubMed: 21795627]

Buckner RL, Vincent JL. Unrest at rest: default activity and spontaneous network correlations. Neuroimage. 2007; 37:1091–6. discussion 1097–9. doi:10.1016/j.neuroimage.2007.01.010. [PubMed: 17368915]

Christian KM, Thompson RF. Neural substrates of eyeblink conditioning: acquisition and retention. Learn. Mem. 2003; 10:427–55. doi:10.1101/lm.59603. [PubMed: 14657256]

Church JA, Fair DA, Dosenbach NUF, Cohen AL, Miezin FM, Petersen SE, Schlaggar BL. Control networks in paediatric Tourette syndrome show immature and anomalous patterns of functional connectivity. Brain. 2009; 132:225–38. doi:10.1093/brain/awn223. [PubMed: 18952678]

Cox RW. AFNI: software for analysis and visualization of functional magnetic resonance neuroimages. Comput. Biomed. Res. 1996; 29:162–73. [PubMed: 8812068]

Damoiseaux JS, Prater KE, Miller BL, Greicius MD. Functional connectivity tracks clinical deterioration in Alzheimer's disease. Neurobiol. Aging. 2012; 33:828, e19–30. doi:10.1016/j.neurobiolaging.2011.06.024. [PubMed: 21840627]

Damoiseaux JS, Rombouts SARB, Barkhof F, Scheltens P, Stam CJ, Smith SM, Beckmann CF. Consistent resting-state networks across healthy subjects. Proc. Natl. Acad. Sci. U. S. A. 2006; 103:13848–53. doi:10.1073/pnas.0601417103. [PubMed: 16945915]

Deci S, Lemieux SK, Smith-Bell CA, Sparks DL, Schreurs BG. Cholesterol increases ventricular volume in a rabbit model of Alzheimer's disease. J. Alzheimers. Dis. 2012; 29:283–92. doi:10.3233/JAD-2011-111415. [PubMed: 22232012]

Dobromyslin VI, Salat DH, Fortier CB, Leritz EC, Beckmann CF, Milberg WP, McGlinchey RE. Distinct functional networks within the cerebellum and their relation to cortical systems assessed with independent component analysis. Neuroimage. 2012; 60:2073–85. doi:10.1016/j.neuroimage.2012.01.139. [PubMed: 22342804]

Evarts EV, Thach WT. Motor mechanisms of the CNS: cerebrocerebellar interrelations. Annu. Rev. Physiol. 1969; 31:451–98. doi:10.1146/annurev.ph.31.030169.002315. [PubMed: 4885774]

Fair DA, Nigg JT, Iyer S, Bathula D, Mills KL, Dosenbach NUF, Schlaggar BL, Mennes M, Gutman D, Bangaru S, Buitelaar JK, Dickstein DP, Di Martino A, Kennedy DN, Kelly C, Luna B, Schweitzer JB, Velanova K, Wang Y-F, Mostofsky S, Castellanos FX, Milham MP. Distinct neural signatures detected for ADHD subtypes after controlling for micro-movements in resting state functional connectivity MRI data. Front. Syst. Neurosci. 2012; 6:80. doi:10.3389/fnsys.2012.00080. [PubMed: 23382713]

Filippini N, MacIntosh BJ, Hough MG, Goodwin GM, Frisoni GB, Smith SM, Matthews PM, Beckmann CF, Mackay CE. Distinct patterns of brain activity in young carriers of the APOE-epsilon4 allele. Proc. Natl. Acad. Sci. U. S. A. 2009; 106:7209–14. doi:10.1073/pnas.0811879106. [PubMed: 19357304]

Fox MD, Buckner RL, White MP, Greicius MD, Pascual-Leone A. Efficacy of transcranial magnetic stimulation targets for depression is related to intrinsic functional connectivity with the subgenual cingulate. Biol. Psychiatry. 2012; 72:595–603. doi:10.1016/j.biopsych.2012.04.028. [PubMed: 22658708]

Fox MD, Greicius M. Clinical applications of resting state functional connectivity. Front. Syst. Neurosci. 2010; 4:19. doi:10.3389/fnsys.2010.00019. [PubMed: 20592951]

Girgis, M.; Shih-Chang, W. A new stereotaxic atlas of the rabbit brain. Warren H. Green, Inc.; St. Louis, Mo.: 1981.

Gould HJ. Body surface maps in the somatosensory cortex of rabbit. J. Comp. Neurol. 1986; 243:207–33. doi:10.1002/cne.902430206. [PubMed: 3944277]

Greene DJ, Laumann TO, Dubis JW, Ihnen SK, Neta M, Power JD, Pruett JR, Black KJ, Schlaggar BL. Developmental changes in the organization of functional connections between the basal ganglia and cerebral cortex. J. Neurosci. 2014; 34:5842–54. doi:10.1523/JNEUROSCI.3069-13.2014. [PubMed: 24760844]

Greicius MD, Srivastava G, Reiss AL, Menon V. Default-mode network activity distinguishes Alzheimer's disease from healthy aging: evidence from functional MRI. Proc. Natl. Acad. Sci. U. S. A. 2004; 101:4637–42. doi:10.1073/pnas.0308627101. [PubMed: 15070770]

Hall SS, Jiang H, Reiss AL, Greicius MD. Identifying large-scale brain networks in fragile X syndrome. JAMA psychiatry. 2013; 70:1215–23. doi:10.1001/jamapsychiatry.2013.247. [PubMed: 24068330]

Hampson M, Driesen NR, Skudlarski P, Gore JC, Constable RT. Brain connectivity related to working memory performance. J. Neurosci. 2006; 26:13338–43. doi:10.1523/JNEUROSCI.3408-06.2006. [PubMed: 17182784]

Hattori S, Chen L, Weiss C, Disterhoft JF. Robust hippocampal responsivity during retrieval of consolidated associative memory. Hippocampus. 2014a doi:10.1002/hipo.22401.

Hattori S, Yoon T, Disterhoft JF, Weiss C. Functional reorganization of a prefrontal cortical network mediating consolidation of trace eyeblink conditioning. J. Neurosci. 2014b; 34:1432–45. doi:10.1523/JNEUROSCI.4428-13.2014. [PubMed: 24453332]

Hughes A, Vaney DI. The organization of binocular cortex in the primary visual area of the rabbit. J. Comp. Neurol. 1982; 204:151–64. doi:10.1002/cne.902040205. [PubMed: 6276448]

Hutchison RM, Leung LS, Mirsattari SM, Gati JS, Menon RS, Everling S. Resting-state networks in the macaque at 7 T. Neuroimage. 2011; 56:1546–55. doi:10.1016/j.neuroimage.2011.02.063. [PubMed: 21356313]

Hutchison RM, Mirsattari SM, Jones CK, Gati JS, Leung LS. Functional networks in the anesthetized rat brain revealed by independent component analysis of resting-state FMRI. J. Neurophysiol. 2010; 103:3398–406. doi:10.1152/jn.00141.2010. [PubMed: 20410359]

Jonckers E, Van Audekerke J, De Visscher G, Van der Linden A, Verhoye M. Functional connectivity fMRI of the rodent brain: Comparison of functional connectivity networks in rat and mouse. PLoS One. 2011; 6:e18876. doi:10.1371/journal.pone.0018876. [PubMed: 21533116]

Kelly RM, Strick PL. Cerebellar loops with motor cortex and prefrontal cortex of a nonhuman primate. J. Neurosci. 2003; 23:8432–44. [PubMed: 12968006]

Kemp JM, Powell TP. The connexions of the striatum and globus pallidus: synthesis and speculation. Philos. Trans. R. Soc. Lond. B. Biol. Sci. 1971; 262:441–57. [PubMed: 4399123]

Kuroda M, Yokofujita J, Oda S, Price JL. Synaptic relationships between axon terminals from the mediodorsal thalamic nucleus and gamma-aminobutyric acidergic cortical cells in the prelimbic cortex of the rat. J. Comp. Neurol. 2004; 477:220–34. doi:10.1002/cne.20249. [PubMed: 15300791]

Lehmann M, Madison CM, Ghosh PM, Seeley WW, Mormino E, Greicius MD, Gorno-Tempini ML, Kramer JH, Miller BL, Jagust WJ, Rabinovici GD. Intrinsic connectivity networks in healthy subjects explain clinical variability in Alzheimer's disease. Proc. Natl. Acad. Sci. U. S. A. 2013; 110:11606–11. doi:10.1073/pnas.1221536110. [PubMed: 23798398]

Lewis CM, Baldassarre A, Committeri G, Romani GL, Corbetta M. Learning sculpts the spontaneous activity of the resting human brain. Proc. Natl. Acad. Sci. U. S. A. 2009; 106:17558–63. doi:10.1073/pnas.0902455106. [PubMed: 19805061]

Li L, Weiss C, Disterhoft JF, Wyrwicz AM. Functional magnetic resonance imaging in the awake rabbit: a system for stimulus presentation and response detection during eyeblink conditioning. J. Neurosci. Methods. 2003; 130:45–52. [PubMed: 14583403]

Liang Z, King J, Zhang N. Uncovering Intrinsic Connectional Architecture of Functional Networks in Awake Rat Brain. J. Neurosci. 2011; 31:3776–3783. doi:10.1523/JNEUROSCI.4557-10.2011. [PubMed: 21389232]

Liu QY, Bingham EJ, Twine SM, Geiger JD, Ghribi O. Metabolomic Identification in Cerebrospinal Fluid of the Effects of High Dietary Cholesterol in a Rabbit Model of Alzheimer's Disease. Metabolomics open access. 2012; 2:109. [PubMed: 24851192]

Liu JV, Hirano Y, Nascimento GC, Stefanovic B, Leopold DA, Silva AC. fMRI in the awake marmoset: somatosensory-evoked responses, functional connectivity, and comparison with propofol anesthesia. Neuroimage. 2013; 78:186–95. doi:10.1016/j.neuroimage.2013.03.038. [PubMed: 23571417]

Liu X, Zhu X-H, Zhang Y, Chen W. The change of functional connectivity specificity in rats under various anesthesia levels and its neural origin. Brain Topogr. 2013; 26:363–77. doi:10.1007/s10548-012-0267-5. [PubMed: 23208517]

Lu H, Zou Q, Gu H, Raichle ME, Stein EA, Yang Y. Rat brains also have a default mode network. Proc. Natl. Acad. Sci. U. S. A. 2012; 109:3979–84. doi:10.1073/pnas.1200506109. [PubMed: 22355129]

Lustig C, Snyder AZ, Bhakta M, O'Brien KC, McAvoy M, Raichle ME, Morris JC, Buckner RL. Functional deactivations: change with age and dementia of the Alzheimer type. Proc. Natl. Acad. Sci. U. S. A. 2003; 100:14504–9. doi:10.1073/pnas.2235925100. [PubMed: 14608034]

Mackey AP, Miller Singley AT, Bunge SA. Intensive reasoning training alters patterns of brain connectivity at rest. J. Neurosci. 2013; 33:4796–803. doi:10.1523/JNEUROSCI.4141-12.2013. [PubMed: 23486950]

Mantini D, Corbetta M, Romani GL, Orban GA, Vanduffel W. Evolutionarily Novel Functional Networks in the Human Brain? J. Neurosci. 2013; 33:3259–3275. doi:10.1523/JNEUROSCI.4392-12.2013. [PubMed: 23426655]

Mantini D, Gerits A, Nelissen K, Durand J-B, Joly O, Simone L, Sawamura H, Wardak C, Orban GA, Buckner RL, Vanduffel W. Default mode of brain function in monkeys. J. Neurosci. 2011; 31:12954–62. doi:10.1523/JNEUROSCI.2318-11.2011. [PubMed: 21900574]

McLeod KR, Langevin LM, Goodyear BG, Dewey D. Functional connectivity of neural motor networks is disrupted in children with developmental coordination disorder and attention-deficit/hyperactivity disorder. NeuroImage. Clin. 2014; 4:566–75. doi:10.1016/j.nicl.2014.03.010. [PubMed: 24818082]

Medina JF, Repa JC, Mauk MD, LeDoux JE. Parallels between cerebellum- and amygdala-dependent conditioning. Nat. Rev. Neurosci. 2002; 3:122–31. doi:10.1038/nrn728. [PubMed: 11836520]

Muñoz-Moreno E, Arbat-Plana A, Batalle D, Soria G, Illa M, Prats-Galino A, Eixarch E, Gratacos E. A magnetic resonance image based atlas of the rabbit brain for automatic parcellation. PLoS One. 2013; 8:e67418. doi:10.1371/journal.pone.0067418. [PubMed: 23844007]

Nasrallah FA, Tan J, Chuang K-H. Pharmacological modulation of functional connectivity: α2-adrenergic receptor agonist alters synchrony but not neural activation. Neuroimage. 2012; 60:436–46. doi:10.1016/j.neuroimage.2011.12.026. [PubMed: 22209807]

O'Reilly JX, Croxson PL, Jbabdi S, Sallet J, Noonan MP, Mars RB, Browning PGF, Wilson CRE, Mitchell AS, Miller KL, Rushworth MFS, Baxter MG. Causal effect of disconnection lesions on interhemispheric functional connectivity in rhesus monkeys. Proc. Natl. Acad. Sci. U. S. A. 2013; 110:13982–7. doi:10.1073/pnas.1305062110. [PubMed: 23924609]

Perez-Garmendia R, Hernandez-Zimbron LF, Morales MA, Luna-Muñoz J, Mena R, Nava-Catorce M, Acero G, Vasilevko V, Viramontes-Pintos A, Cribbs DH, Gevorkian G. Identification of N-terminally truncated pyroglutamate amyloid-β in cholesterol-enriched diet-fed rabbit and AD brain. J. Alzheimers. Dis. 2014; 39:441–55. doi:10.3233/JAD-130590. [PubMed: 24240639]

Pessoa L. Understanding brain networks and brain organization. Phys. Life Rev. 2014; 11:400–35. doi:10.1016/j.plrev.2014.03.005. [PubMed: 24819881]

Pizoli CE, Shah MN, Snyder AZ, Shimony JS, Limbrick DD, Raichle ME, Schlaggar BL, Smyth MD. Resting-state activity in development and maintenance of normal brain function. Proc. Natl. Acad. Sci. U. S. A. 2011; 108:11638–43. doi:10.1073/pnas.1109144108. [PubMed: 21709227]

Power JD, Cohen AL, Nelson SM, Wig GS, Barnes KA, Church JA, Vogel AC, Laumann TO, Miezin FM, Schlaggar BL, Petersen SE. Functional network organization of the human brain. Neuron. 2011; 72:665–78. doi:10.1016/j.neuron.2011.09.006. [PubMed: 22099467]

Power JD, Fair DA, Schlaggar BL, Petersen SE. The development of human functional brain networks. Neuron. 2010; 67:735–48. doi:10.1016/j.neuron.2010.08.017. [PubMed: 20826306]

Raichle ME, MacLeod AM, Snyder AZ, Powers WJ, Gusnard DA, Shulman GL. A default mode of brain function. Proc. Natl. Acad. Sci. U. S. A. 2001; 98:676–82. doi:10.1073/pnas.98.2.676. [PubMed: 11209064]

Sawyer CH, Everett JW, Green JD. The rabbit diencephalon in stereotaxic coordinates. J. Comp. Neurol. 1954; 101:801–24. [PubMed: 13233360]

Schmahmann JD, Pandya DN. The cerebrocerebellar system. Int. Rev. Neurobiol. 1997; 41:31–60. [PubMed: 9378595]

Schreurs BG, Smith-Bell CA, Lemieux SK. Dietary cholesterol increases ventricular volume and narrows cerebrovascular diameter in a rabbit model of Alzheimer's disease. Neuroscience. 2013; 254:61–9. doi:10.1016/j.neuroscience.2013.09.015. [PubMed: 24045100]

Seeley WW, Crawford RK, Zhou J, Miller BL, Greicius MD. Neurodegenerative diseases target large-scale human brain networks. Neuron. 2009; 62:42–52. doi:10.1016/j.neuron.2009.03.024. [PubMed: 19376066]

Shambes GM, Gibson JM, Welker W. Fractured somatotopy in granule cell tactile areas of rat cerebellar hemispheres revealed by micromapping. Brain. Behav. Evol. 1978; 15:94–140. [PubMed: 638731]

Shibata H, Honda Y. Thalamocortical projections of the anterodorsal thalamic nucleus in the rabbit. J. Comp. Neurol. 2012; 520:2647–56. doi:10.1002/cne.23057. [PubMed: 22314639]

Shirer WR, Ryali S, Rykhlevskaia E, Menon V, Greicius MD. Decoding subject-driven cognitive states with whole-brain connectivity patterns. Cereb. Cortex. 2012; 22:158–65. doi:10.1093/cercor/bhr099. [PubMed: 21616982]

Smith SM, Fox PT, Miller KL, Glahn DC, Fox PM, Mackay CE, Filippini N, Watkins KE, Toro R, Laird AR, Beckmann CF. Correspondence of the brain's functional architecture during activation and rest. Proc. Natl. Acad. Sci. U. S. A. 2009; 106:13040–5. doi:10.1073/pnas.0905267106. [PubMed: 19620724]

Smith SM, Miller KL, Moeller S, Xu J, Auerbach EJ, Woolrich MW, Beckmann CF, Jenkinson M, Andersson J, Glasser MF, Van Essen DC, Feinberg DA, Yacoub ES, Ugurbil K. Temporally-independent functional modes of spontaneous brain activity. Proc. Natl. Acad. Sci. U. S. A. 2012; 109:3131–6. doi:10.1073/pnas.1121329109. [PubMed: 22323591]

Sporns O. Contributions and challenges for network models in cognitive neuroscience. Nat. Neurosci. 2014; 17:652–60. doi:10.1038/nn.3690. [PubMed: 24686784]

Stein T, Moritz C, Quigley M, Cordes D, Haughton V, Meyerand E. Functional Connectivity in the Thalamus and Hippocampus Studied with Functional MR Imaging. AJNR Am J Neuroradiol. 2000; 21:1397–1401. [PubMed: 11003270]

Strick PL. How do the basal ganglia and cerebellum gain access to the cortical motor areas? Behav. Brain Res. 1985; 18:107–123. doi:10.1016/0166-4328(85)90067-1. [PubMed: 3913443]

Supekar K, Menon V, Rubin D, Musen M, Greicius MD. Network analysis of intrinsic functional brain connectivity in Alzheimer's disease. PLoS Comput. Biol. 2008; 4:e1000100. doi:10.1371/journal.pcbi.1000100. [PubMed: 18584043]

Tambini A, Ketz N, Davachi L. Enhanced brain correlations during rest are related to memory for recent experiences. Neuron. 2010; 65:280–90. doi:10.1016/j.neuron.2010.01.001. [PubMed: 20152133]

Urban, I.; Richard, P. A stereotaxic atlas of the New Zealand rabbit's brain. Charles C. Thomas; Springfield, IL.: 1972.

Vincent JL, Patel GH, Fox MD, Snyder AZ, Baker JT, Van Essen DC, Zempel JM, Snyder LH, Corbetta M, Raichle ME. Intrinsic functional architecture in the anaesthetized monkey brain. Nature. 2007; 447:83–6. doi:10.1038/nature05758. [PubMed: 17476267]

Weiss C, Disterhoft JF. Exploring prefrontal cortical memory mechanisms with eyeblink conditioning. Behav. Neurosci. 2011; 125:318–26. doi:10.1037/a0023520. [PubMed: 21517143]

Wyrwicz AM, Chen N, Li L, Weiss C, Disterhoft JF. fMRI of visual system activation in the conscious rabbit. Magn. Reson. Med. 2000; 44:474–8. [PubMed: 10975901]

Yu Q, Allen EA, Sui J, Arbabshirani MR, Pearlson G, Calhoun VD. Brain connectivity networks in schizophrenia underlying resting state functional magnetic resonance imaging. Curr. Top. Med. Chem. 2012; 12:2415–25. [PubMed: 23279180]

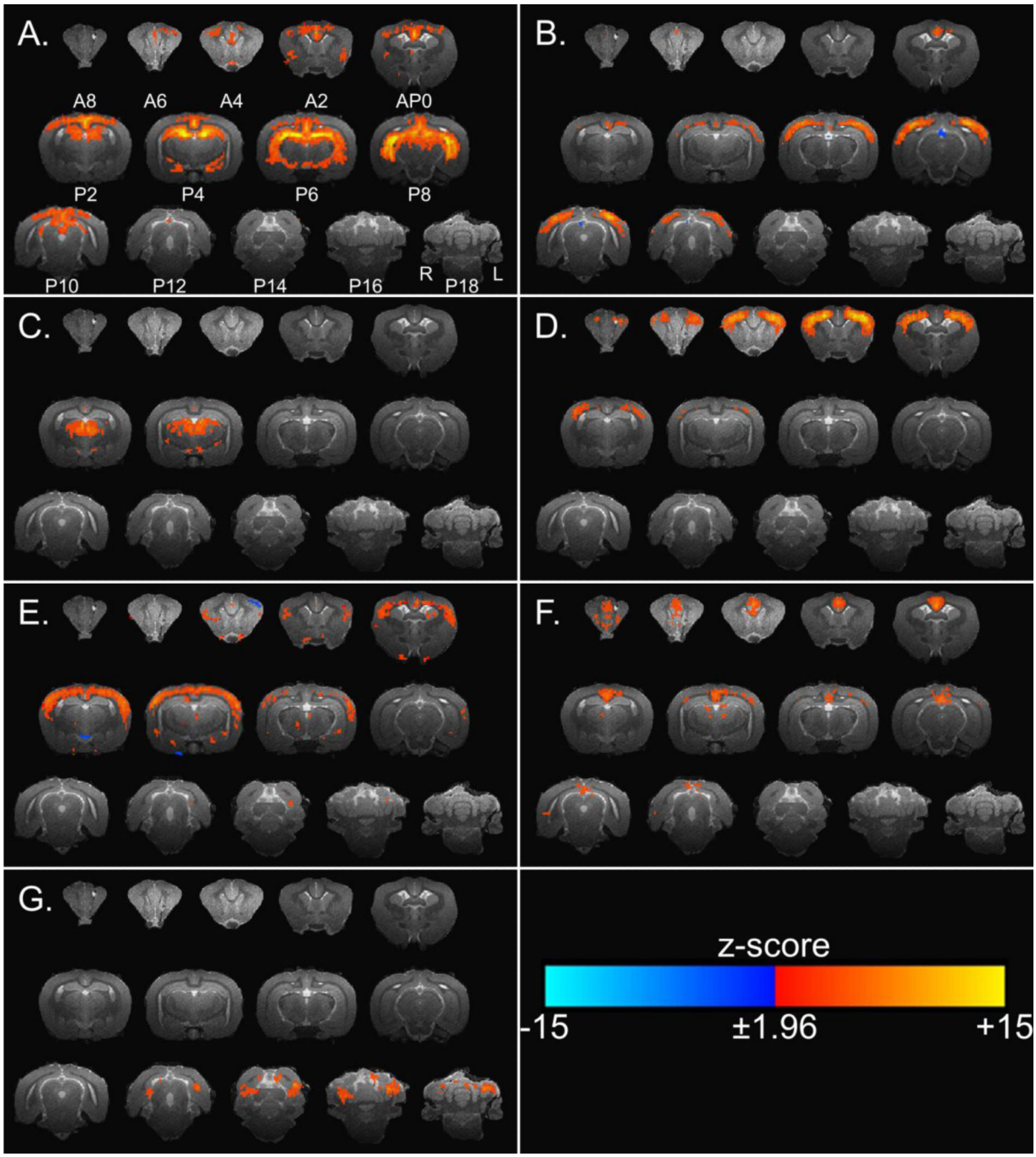

Figure 1.

Intrinsic connectivity networks of the rabbit brain identified using MELODIC group ICA. **A.** Component C1, Hippocampal network; **B.** C2, visual network; **C.** C3, thalamic network; **D.** C4, sensorimotor network; **E.** C5, parietal cortical network; **F.** C6, default mode network; **G.** C11, cerebellar network. Color bar represents the z-score of each component.

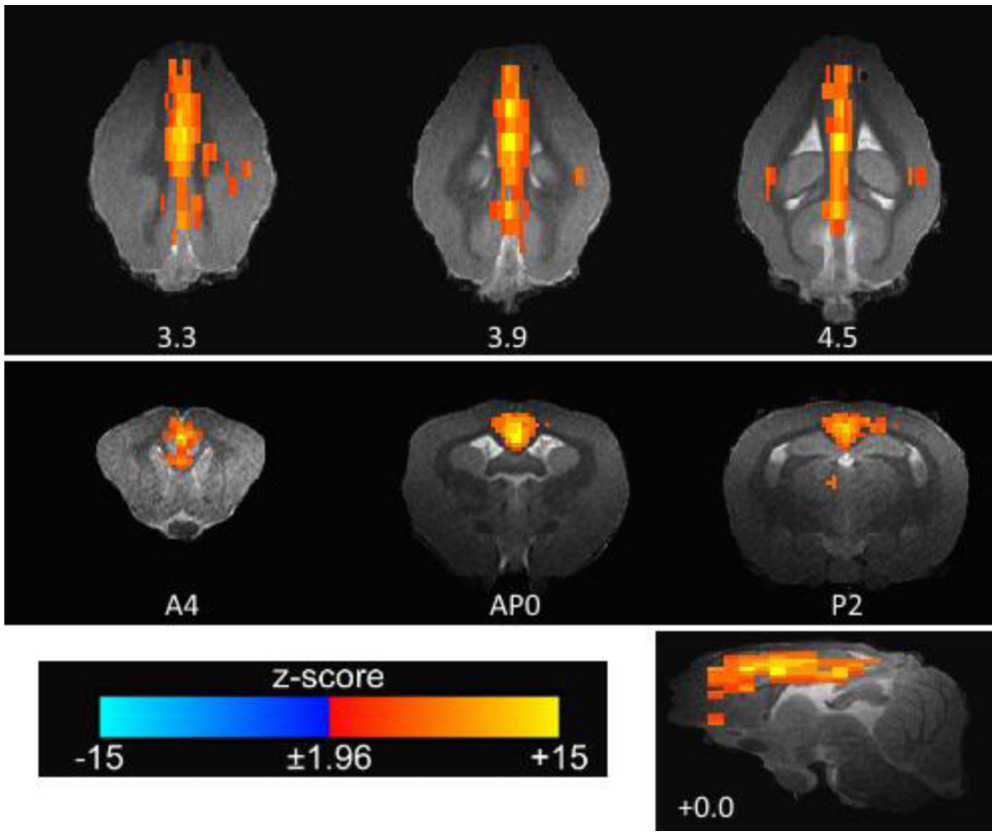

Figure 2.
Default mode network in rabbits. Component C6 with axial, coronal, and sagittal slices at the given coordinates. Color bar represents the z-score of the default mode component.

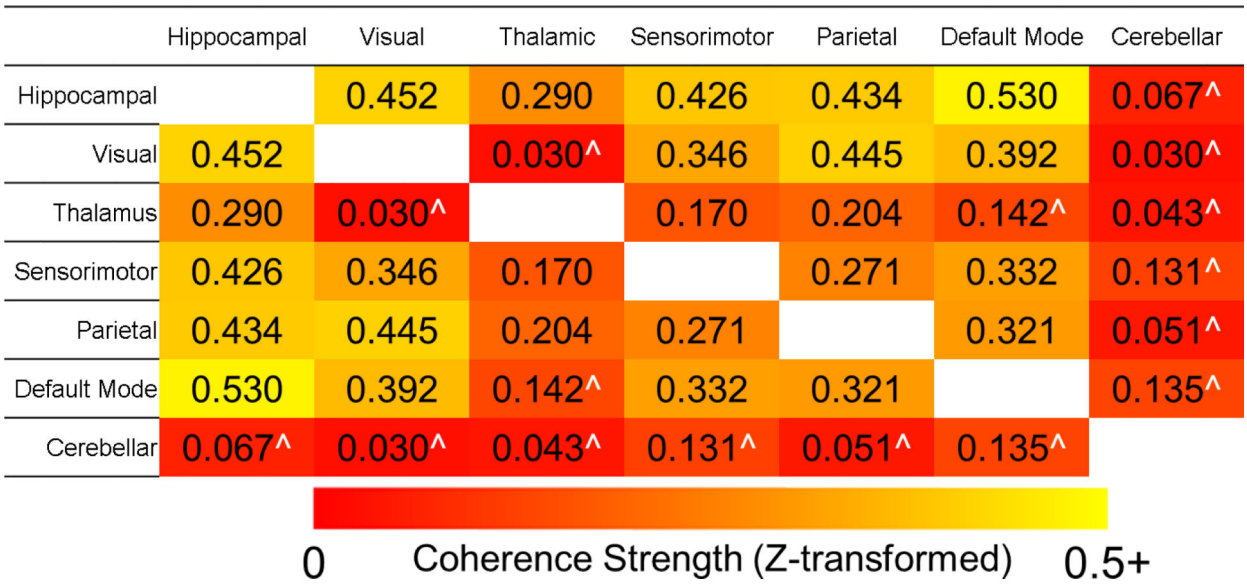

Figure 3.

Coherence strength between each of the 7 networks. Component time-courses for each subject were cross-correlated with every other component time-course, Z-transformed and averaged across the twelve rabbits. Red-to-yellow color scale is meant as a guide to the reader's eye. All coherence comparisons are significantly different from zero unless otherwise labeled with a "^".

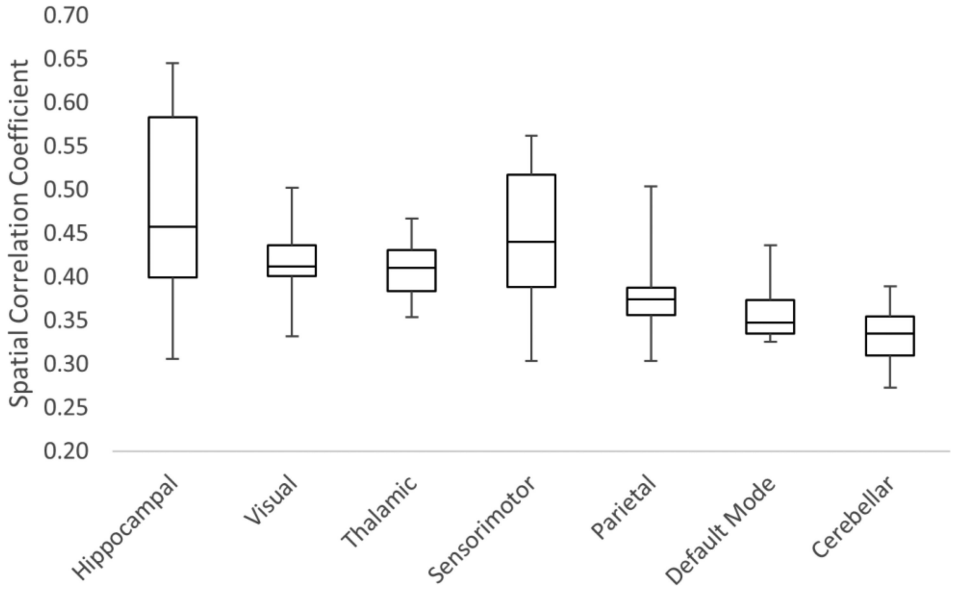

Figure 4.

Box plot of spatial correlation coefficients between the group-level ICA components and individual subject components produced after dual regression.

Table 1

Seven intrinsic networks identified in the awake rabbit

ICA network map component	Functional network description
C1 (Fig. 1A)	Hippocampal
C2 (Fig. 1B)	Visual
C3 (Fig. 1C)	Thalamic
C4 (Fig. 1D)	Sensorimotor
C5 (Fig. 1E)	Parietal
C6 (Fig. 1F)	Default Mode
C11 (Fig. 1G)	Cerebellar